Mitigating the Energy Impacts of VBTI Aging in Photonic Networks-on-Chip Architectures with Multilevel Signaling

Ishan G Thakkar
Department of Electrical and Computer Engineering
University of Kentucky, Lexington, KY, USA
igthakkar@uky.edu

Sudeep Pasricha
Department of Electrical and Computer Engineering
Colorado State University, Fort Collins, CO, USA
sudeep@colostate.edu

***Abstract*—Photonic networks-on-chip (PNoCs) can enable higher bandwidth and lower latency data transfers at the speed of light. Such PNoCs consist of photonic waveguides with dense-wavelength-division-multiplexing (DWDM) for signal traversal and microring resonators (MRs) for signal modulation and reception. To enable MRs to modulate and receive DWDM photonic signals, change in the free-carrier concentration in or operating temperature of MRs through their voltage biasing is essential. But long-term operation of MRs with constant or time-varying temperature and voltage biasing causes aging. Such voltage bias and temperature induced (VBTI) aging in MRs leads to resonance wavelength drifts and Q-factor degradation at the device-level, which in turn exacerbates three key spectral effects at the photonic link level, namely the intermodulation crosstalk, heterodyne crosstalk, and signal sidelobes truncation. These adverse spectral effects ultimately increase signal power attenuation and energy-per-bit in PNoCs. Our frequency-domain analysis of photonic links shows that the use of the four pulse amplitude modulation (4-PAM) signaling instead of the traditional on-off keying (OOK) signaling can proactively reduce signal attenuation caused by the VBTI aging induced spectral effects. Our system-level evaluation results indicate that, compared to OOK based PNoCs with no aging, 4-PAM based PNoCs can achieve 5.5% better energy-efficiency even after undergoing VBTI aging for 3 Years.**

Keywords-photonic networks-on-chip, crosstalk, aging, frequency domain, resonance passband

I. INTRODUCTION

To meet the inter-core communication demand of the state-of-the-art manycore chips, the use of electrical networks-on-chip (ENoCs) has become a norm [1]. However, with ever increasing core count, the performance and energy-efficiency of such ENoCs are projected to scale poorly. Due to recent advances in the silicon photonic interconnects technology, photonic NoCs (PNoCs) are being considered as a potential solution to overcome the drawbacks of traditional ENoCs [2]. It is because PNoCs can provide several prolific advantages over traditional ENoCs, including near light speed transfers, high bandwidth density, and low dynamic power dissipation [3]. These advantages of PNoCs have catalyzed research for their integration in future manycore systems.

The basic building blocks of PNoC architectures (e.g., [4]-[8]) are photonic links. Typically, a photonic link connects two or more nodes of the PNoC and employs multiple photonic waveguides and microring resonator (MR) devices as its key components. A photonic waveguide typically supports dense wavelength division multiplexing (DWDM) of a large number of wavelengths. Each of these wavelengths corresponds to a transmission channel used for data transfers. An MR is a compact and highly wavelength-selective device (i.e., a compact device with a narrow resonance passband), which incorporates a PN-junction in its silicon (Si) core and a microheater in its silicon dioxide (SiO_2) surroundings. The resonance wavelength of an MR can be adjusted by manipulating either the free-carrier concentration in the MR's core through voltage biasing of its PN-junction or the MR's local temperature through voltage biasing of its microheater. This resonance adjustive property of MRs renders them energy-efficiency and promotes their use in PNoC architectures as modulators, receivers, and switches. The MR modulators (that are in resonance with the utilized wavelengths) at the source node modulate electrical signals (i.e., sequence of logical '1' and '0' voltage levels) onto the utilized wavelengths to convert them in photonic signals that travel through the waveguide. MR receivers at the destination node receive photonic signals from the waveguide and recover electrical signals. Moreover, MR switches can route the photonic signals in the PNoC. Thus, DWDM photonic waveguides and wavelength-selective MRs enable high-bandwidth parallel data transfers across the PNoC.

The application of voltage bias across an MR's PN-junction to adjust its resonance generates an electric field across the MR's Si (core) and SiO_2 (cladding) boundary. Similar to MOSFETs, this electric field generates voltage bias temperature induced (VBTI) traps at the Si-SiO_2 boundary of the MR over time (i.e., VBTI aging) [9]. From [9], these VBTI aging induced traps alter carrier concentration in the Si core of MRs, which incur red shifts in the MRs' resonance wavelengths and increase the widths of the MRs' resonance passbands (or decrease the MRs' Q-factor). This VBTI aging induced degradation in the MRs' resonance passbands increases photonic signal degradation and decreases energy-efficiency in PNoCs that utilize these MRs. For example, over a span of 5 years, VBTI aging can increase power penalty of signal degradation in PNoC architectures by up to 7.6dB and energy-delay product by up to 26.8% [9]. A detailed analysis of VBTI aging in MRs and its impacts on PNoCs is presented in [9], *but no prior work till date has focused on mitigating the adverse impacts of VBTI aging in PNoC architectures.*

This paper presents four pulse amplitude modulation (4-PAM) signaling as a means of proactively mitigating the adverse impacts of VBTI aging on the energy-efficiency of PNoC architectures. The motivation of using 4-PAM signaling to counter the energy impacts of aging comes from the fact that 4-PAM signaling based PNoC architectures can achieve significantly better energy-efficiency compared to the traditional on-off keying (OOK) signaling based PNoC architectures [10]. This improved energy-efficiency of 4-PAM based PNoCs is utilized in this paper to provide proactive guard against the adverse impacts of VBTI aging.

978-1-5386-7466-6/18/$31.00 ©2018 IEEE

The key contributions of this paper are summarized below.

- We perform frequency-domain analysis of the photonic link level impacts of VBTI aging. Our analysis shows that the energy impacts of VBTI aging are primarily caused by signal degradation due to aging-induced unsought overlap of photonic signal and MR resonance spectra.
- In our frequency-domain analysis, we also show that use of 4-PAM signaling instead of traditional OOK signaling can reduce signal degradation caused by aging-induced spectral effects.
- We analyze the system-level impacts of VBTI aging on two variants of the well-known CLOS PNoC architecture [4] and show that the 4-PAM signaling based CLOS PNoC architecture yields better energy-efficiency than the OOK signaling based CLOS PNoC after 5 years of aging.

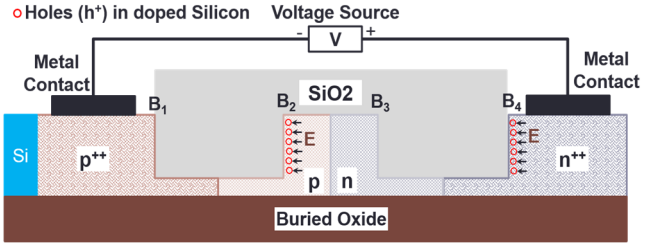

Fig. 1: Cross-section of a tunable MR with PN junction in its core to facilitate carrier injection and depletion with voltage biasing.

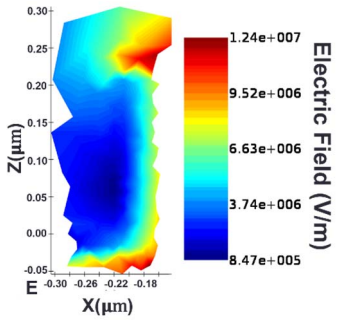

Fig. 2: Distribution of electric field (E) across Si-SiO$_2$ boundary B$_2$ when -4V bias voltage is applied across PN junction.

II. VBTI Aging in MRs

To understand the mechanism of VBTI aging in MRs, consider Fig. 1, which illustrates a typical MR structure with a PN-junction in its Si core that is cladded by SiO_2 surroundings. To impart high-speed and low-power resonance adjustive property to the MR, its PN-junction needs to be reverse (or negatively) biased [11], which is accomplished by applying higher voltage on the n side of the PN-junction (Fig. 1). When a negative voltage is applied across the PN junction of the MR, an electric field 'E' is generated from right to left across the Si-SiO_2 boundaries B1, B2, B3, and B4 (Fig. 1). We used the Lumerical Solutions DEVICE [12] tool to construct and model the PN junction of an MR. For our preliminary analysis, we consider an MR waveguide similar to the one reported in [13] with a radius of 2µm, fabricated using standard Si-SiO_2 material with a core cross-section of 450nm × 250nm. We simulated the MR using the charge transport solver in the DEVICE tool and then obtained the distribution of electric field across the MR waveguide with a bias voltage of -4V. The results from the DEVICE tool demonstrate the presence of electric field E across all the Si-SiO_2 boundaries (i.e., B1, B2, B3, and B4). This electric field present across the Si-SiO_2 boundaries B2 (shown in Fig. 2(b)) and B4 attracts holes towards them (Fig.1) and generates traps across these boundaries similar to pMOSFETs [14]. These voltage bias induced traps on the B2 boundary change the electro-optic dynamics of the MR with time, which causes aging in the MR.

A. Analytical Models for VBTI Aging Mechanism

Several works in the literature (e.g., [14]-[16]) use reaction-diffusion (RD) models to characterize boundary trap generation at the MOSFET Si-SiO_2 boundary. As boundary traps in MR's are similar to boundary traps in MOSFETs, we use the same RD model to simulate the boundary trap generation at the MR's Si-SiO_2 boundary. This trap generation mechanism is represented as a chemical reaction in Eq. (1), where holes (h+) in the MR's Si core weaken a Si–H bond and hydrogen (H) is detached [15] in the presence of electric field (E_B) and thermal variations (ΔT):

$$Si - H + h^+ \overset{\Delta T, E_B}{\Longleftrightarrow} Si^* + H, \tag{1}$$

The generated Si dangling bond (Si*) acts as a donor-like boundary trap. The H ion released from the bond can diffuse away from the Si-SiO_2 boundary or anneal an existing trap. At any given time, the boundary trap density (N_{BT}) depends on the Si-H bond breaking rate k_F, Si-H bond annealing rate k_R, Si-H bond density available before stress (N_0), and the hydrogen (H) density at the MR's Si-SiO_2 boundary (N_H) through the following equations, the detailed description of which can be found in [9].

$$N_{BT} N_H = k_F N_0 / k_R, \tag{2}$$

$$k_F = B\sigma_0 E_{ox} e^{\frac{E_{ox}}{E_0}} e^{\frac{-E_F}{K_B T}}, \tag{3}$$

$$k_R = k_{R0} e^{\frac{-E_R}{K_B T}}, \tag{4}$$

In the above equations, E_F is activation energy of forward bond dissociation, E_R is activation energy of reverse bond annealing, K_B is the Boltzmann constant, E_{ox} is electric field strength across Si-SiO_2 boundary induced due to voltage biasing, $\exp(E_{ox}/E_0)$ is the field dependent tunneling of holes into SiO_2 cladding, σ_0 is the capture cross-section of the Si–H bonds, T is operating temperature, and B determines field dependence of the Si–H bond dissociation. It is evident from these modeling equations that the rate of boundary trap generation and hence the boundary trap density N_{BT} depends on the electric field strength across Si-SiO_2 boundary E_{ox} and operating temperature T. Because of this dependence, elevated levels of boundary electric field E_{ox} (or voltage bias) and temperature T accelerate boundary trap generation, which in turn accelerates MR aging.

The presence of fabrication process and temperature variations across different MRs of a PNoC and the need of compensating for these variations make the use of elevated levels of voltage bias and temperature with the MRs inevitable. Fabrication process and temperature variations cause drifts in MRs' resonance wavelengths, which must be rectified for error-free and low-overhead operation of the MRs. From [17] and [18], to remedy these variations induced resonance drifts in MRs, use of elevated (or altered) levels of voltage bias and/or temperature with the MRs is inevitable. These elevated (or altered) levels of

voltage bias and temperature are likely to accelerate boundary trap generation in the MRs. Therefore, MRs of a PNoC are likely to be inflicted by VBTI aging and its adverse impacts.

III. Impacts of VBTI Aging

The VBTI aging induced boundary traps change the electro-optic dynamics and resonance characteristics of MRs with time, which in turn deteriorates the energy-efficiency of PNoCs that utilize these MRs. In this section, we provide detailed analysis of the impacts of VBTI aging.

A. Impacts of Aging on MRs' Resonance Characteristics

The VBTI aging induced boundary traps in an MR ultimately affects the MR's resonance characteristics in two ways: 1) induce red shift in the MR's resonance, and 2) increase the width of the MR's resonance passband (or decrease the MR's Q-factor). With the onset of boundary trap generation, the concentration of holes in an aging affected MR's core decreases, which increases the MR core's refractive index. However, the refractive index of the MR's SiO_2 surroundings remains relatively unaltered. Consequently, the refractive index contrast between the MR's core and surroundings, along with the MR's effective refractive index increases. The increase in the MR's effective refractive index induces red shift in its resonance passband. On the other hand, the increase in the refractive index contrast between the MR's core and surroundings increases optical scattering loss in the MR's cavity, which in turn decreases the MR's Q-factor (i.e., increases the MR's passband width).

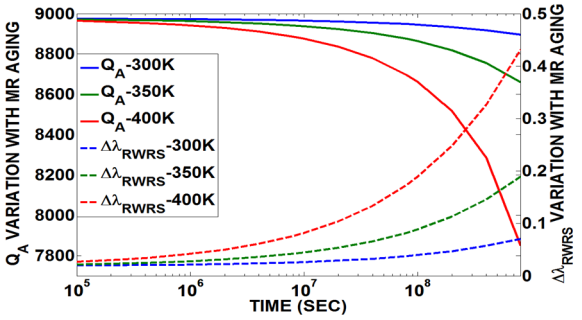

Fig. 3: Variation of resonance wavelength red shift ($\Delta\lambda_{RWRS}$) and Q_A with time at three operating temperatures 300K, 350K, and 400K.

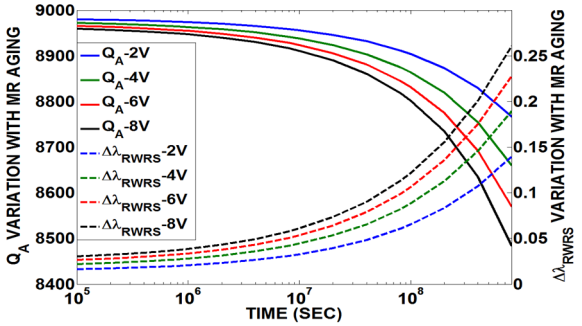

Fig. 4: Variation of Q_A and resonance wavelength red shift ($\Delta\lambda_{RWRS}$) with operation time at four bias voltages -2V, -4V, -6V, and -8V.

Using the analytical models for VBTI aging and the design parameters of an example MR presented in [9], we evaluated the change in the example MR's resonance characteristics (red shift in resonance and Q-factor) with aging for different levels of bias voltage and operating temperature. For this evaluation, we adopted the initial resonance characteristic of the example MR from [9]. Fig. 3 shows the variation in resonance wavelength red shift ($\Delta\lambda_{RWRS}$) and Q-factor (Q_A) with aging in MRs at different temperatures: 300K, 350K, and 400K. Moreover, Fig. 4 shows $\Delta\lambda_{RWRS}$ and Q_A with aging in MRs at different levels of negative voltage bias: -2V, -4V, -6V, and -8V. From Fig. 3 and Fig. 4, at a particular temperature and bias level, with the increase in MR aging (i.e., increase in usage time) $\Delta\lambda_{RWRS}$ increases and Q_A decreases. Moreover, it can also be observed from Fig. 3 and Fig. 4 that the rates of change in $\Delta\lambda_{RWRS}$ and Q_A increase with increase in temperature or voltage bias level. *Thus, it can be concluded from Fig. 3 and Fig. 4 that higher operating temperatures and voltage bias levels accelerate VBTI aging in MRs.*

B. Impacts of Aging on DWDM-Based OOK Links

A DWDM-based point-to-point OOK link supports parallel transfer of multiple OOK-modulated DWDM signals from a source node to a destination node through a photonic waveguide. The source node employs multiple modulator MRs to modulate the utilized DWDM wavelengths available in the waveguide, whereas the destination node employs multiple receiver MRs to receive the modulated DWDM signals from the waveguide. As VBTI aging primarily affects MRs' spectral (i.e., resonance) characteristics and MRs are primarily employed at the source and destination nodes of an OOK link, the impacts of VBTI aging on the link can be best explained using frequency domain (i.e., spectral) representation of the source and destination nodes.

1) VBTI Aging in Modulator MRs of Source Node

Consider Fig. 5 which illustrates an example source node in frequency domain before (Fig. 5(a)) and after (Fig. 5(b)) aging. From the figure, all four modulator MRs are represented in frequency domain as Lorentzian frequency/wavelength passbands that are centered on the MRs' resonance frequencies/wavelengths. Similarly, unmodulated wavelength signals are represented as narrow-band frequency spectra that are identical to regularized Dirac-delta functions. From Fig. 5(a), in an ideal scenario before aging, the unmodulated signals' spectra perfectly coincide with the modulator MRs' resonance wavelengths (i.e., centers of the MRs' resonance passbands). In this ideal case, the modulator MRs can modulate the utilized wavelength signals in OOK format efficiently. However, after aging, due to the induced red shifts in the modulator MRs' resonances and the increase in their passband widths, the signal spectra no longer perfectly coincide with the MRs' resonance wavelengths (Fig. 5(b)). As a result, the modulator MRs cannot modulate the utilized wavelength signals efficiently. The inefficient modulation of the utilized wavelengths increases intermodulation crosstalk, which results in attenuated average spectral power for the modulated signals. A detailed explanation of and analytical models for the intermodulation crosstalk phenomenon can be found in [19].

2) VBTI Aging in Receiver MRs of Destination Node

Consider Fig. 6 which illustrates an example destination node in frequency domain before (Fig. 6(a)) and after (Fig. 6(b)) aging. From Fig. 6(a), unlike the unmodulated signals' spectra at the source node, the modulated signals' spectra at the destination node have frequency sidelobes, the widths of which depend on the modulation baud rate (i.e., number of level transitions in unit time). Ideally at a destination node, the centers of the modulated signals' spectra coincide with the centers of the receiver MRs' passbands (Fig. 6(a)). In spite of this ideal spectral alignment, the

receiver MRs' passbands do not completely overlap with their respective signals' spectra as intended for efficient filtering and reception of the signals. This incomplete spectral overlap results in signal sidelobes truncation [20]. Moreover, depending on the spacing between the adjacent wavelength channels, the receiver MRs' passbands partially overlap the neighboring non-resonant signals' spectra, which results in off-resonance filtering or heterodyne crosstalk [20]. The combined effect of the signal sidelobes truncation and heterodyne crosstalk phenomena results in signal degradation and attenuation of average spectral power for the filtered/received photonic signals. Typically, while designing OOK links, the channel spacing and the receiver MRs' passband widths are optimized to trade off signal truncation and crosstalk phenomena so that the effective signal degradation is minimized. But after aging, as shown in Fig. 6(b), due to the induced red shifts in the modulator MRs' resonances and the increase in their passband widths, the effects of both signal truncation and crosstalk phenomena become more adverse, which further increases signal degradation. Detailed explanations and analytical models for the signal sidelobe truncation and heterodyne crosstalk phenomena can be found in [21].

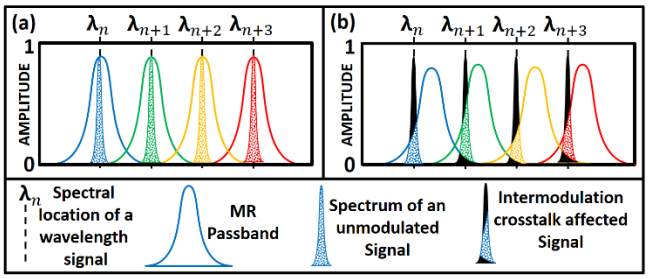

Fig. 5: Illustration of an example source node in frequency domain (a) before aging and (b) after aging.

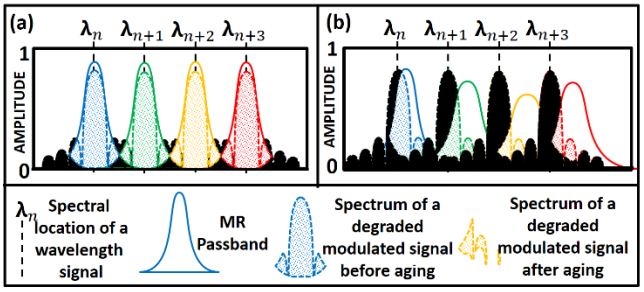

Fig. 6: Illustration of an example destination node in frequency domain (a) before aging and (b) after aging.

Thus, VBTI aging in individual MRs of an OOK link produces three spectral effects: 1) intermodulation crosstalk at the source node, 2) signal sidelobes truncation at the destination node, and 3) heterodyne crosstalk at the destination node. The ultimate impact of these three-fold spectral effects of VBTI aging is power attenuation of the utilized wavelength signals in the OOK link. This signal power attenuation needs to be compensated for to achieve error-free link operation. The predominant way of doing this is to increase the input signal power. But increasing input signal power reduces the energy-efficiency of OOK links and PNoCs that utilize these links. *Hence, the end effect of VBTI aging in MRs is degradation of energy-efficiency in photonic links and PNoCs.*

IV. Mitigating the Impacts of VBTI Aging

As discussed in Section II-A, we cannot avoid VBTI aging of MRs in PNoC architectures, as the causes (i.e., elevated levels of voltage bias and operating temperature) of VBTI aging in PNoC architectures are inevitable. Therefore, to resolve the problem of VBTI aging, the only alternative is to mitigate the adverse impacts of VBTI aging. As the end effect of VBTI aging is degradation of energy-efficiency in PNoCs, any technique or optimization that improves the energy-efficiency of PNoCs can be used to remedy the adverse impacts of VBTI aging. These aging mitigative techniques and optimizations can be reactive or proactive in nature. In this section, we present the four pulse amplitude modulation (4-PAM) signaling as a low-overhead proactive method of mitigating the impacts of VBTI aging.

A. Reactive Mitigation of VBTI Aging Impacts

Mitigation techniques or optimizations that are triggered upon the onset of VBTI aging are referred to as reactive mitigation techniques. Several techniques (e.g. [22]-[26]) presented in prior work can be used to reactively counter the following two device-level effects of VBTI aging on MRs' resonance characteristics: 1) red shift in MRs' resonances and 2) broadening of MRs' resonance passbands. In the remainder of this section, we discuss one by one about mitigating these two device-level effects using reactive mitigation techniques.

The VBTI aging induced red shifts in MR resonances are similar to the variations (i.e., fabrication process and temperature variations [32]) induced red shifts in MR resonances. Therefore, free-carrier injection aka localized trimming, which is a predominantly used technique to counter the variations induced red shifts in MR resonances [17], can also be used to counter the VBTI aging induced red shifts in MR resonances. Localized trimming induces blue shifts in MRs' resonances, which can counter the aging induced resonance red shifts and bring back the MRs' resonances in perfect alignment with the corresponding signals' spectra. This spectral realignment caused by the localized trimming technique eliminates signal sidelobes truncation as one of the link-level spectral effects of VBTI aging. However, from [22], localized trimming can cause additional broadening of the MRs' passbands, which in turn exacerbates the intermodulation crosstalk and heterodyne crosstalk effects of VBTI aging [25]. Nevertheless, dealing with two exacerbated link-level spectral effects is still more manageable than dealing with three link-level spectral effects of VBTI aging. Therefore, *we promote the use of localized trimming to counter the VBTI aging induced red shifts in MR resonances.*

On the other hand, to counter the intermodulation crosstalk and heterodyne crosstalk effects caused by the VBTI aging and localized trimming induced broadening of MRs' resonance passbands, any of the priorly proposed crosstalk mitigation techniques (e.g., [22]-[25]) can be utilized. However, the reactive nature of all these crosstalk mitigation techniques from prior work incur significant performance and/or area overhead. For example, the data-encoding based heterodyne crosstalk mitigation technique presented in [22] can incur performance overhead of up to 20%. Moreover, the crosstalk mitigation technique presented in [25] can incur area overhead of up to 15%. The high overheads of these reactive crosstalk mitigation techniques make them less preferable. *This motivates the need of*

low-overhead techniques that can proactively counter the intermodulation crosstalk and heterodyne crosstalk effects of the VBTI aging induced broadening of MRs' resonance passbands.

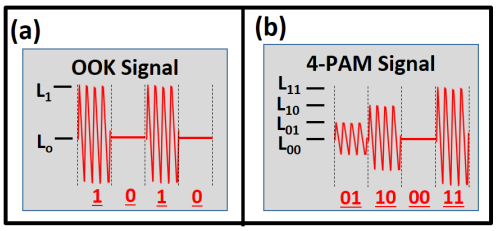

Fig. 7: Illustration of the time-domain representation of (a) on-off-keying (OOK) signaling method and (b) four pulse amplitude modulation (4-PAM) signaling method.

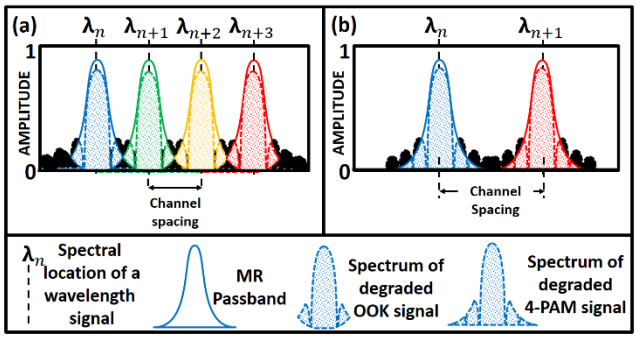

Fig. 8: Illustration of (a) OOK based and (b) 4-PAM based destination nodes in frequency domain.

B. 4-PAM Signaling: A Low-Overhead Technique for Proactive Mitigation of VBTI Aging Impacts

In this section, we present the 4-PAM signaling method as a low-overhead technique that can proactively mitigate the intermodulation crosstalk and heterodyne crosstalk effects of VBTI aging. Fig. 7 illustrates the time-domain representations of a traditional OOK signal and a 4-PAM signal. As evident from the figure, the OOK signal utilizes two optical transmission levels (i.e., L_0 and L_1) to represent one bit of information in one data symbol. On the other hand, the 4-PAM signal utilizes four optical transmission levels (i.e., L_{00}, L_{01}, L_{10}, L_{11}) to represent two bits information in one data symbol. Thus, for a given signal baud-rate (i.e., the number of level transitions in unit time of a data signal), the 4-PAM signaling method achieves 2× bandwidth (or bit-rate) compared to the OOK method.

This ability of doubling the bandwidth without altering the baud-rate of data transmission allows the 4-PAM signaling method to reduce the number of DWDM wavelengths per photonic link by 2× and still achieve the same aggregate link bandwidth as an OOK link. The ability of using 2× less wavelengths allows for 2× wider channel spacing between adjacent wavelength channels. This fact is evident from Fig. 8, which shows the frequency-domain representations of the OOK and 4-PAM signaling based destination nodes. From the figure, the 2× channel spacing and 2× bandwidth with unaltered signal sidelobe widths for 4-PAM signaling (i.e., signal sidelobe widths for OOK and 4-PAM signals of same baud-rate are same) naturally minifies the heterodyne crosstalk effect, as the overlap of the MRs' passbands with the neighboring signals' spectra is reduced. Moreover, it also provides a proactive guard against the exacerbated crosstalk effects caused by VBTI aging induced broadening of MRs' resonance passbands. As a result, 4-PAM based PNoCs can undergo significant aging and still achieve better energy-efficiency compared to OOK based PNoCs with no aging. This fact is corroborated from our evaluation results presented in the next section.

V. EVALUATION

We analyze the adverse impacts of VBTI aging on two variants of the well-known CLOS PNoC architecture [4]. The OOK signaling based variant is referred to as CLOS-OOK PNoC, whereas the 4-PAM signaling based variant is referred to as CLOS-4PAM PNoC.

A. Considered CLOS-Topology PNoC Architecture

We adopt the configuration of the CLOS PNoC from [9]. Each photonic link in the CLOS-OOK PNoC uses 64 DWDM wavelengths between 1525nm-1575nm at 0.8nm channel spacing, with 32 wavelengths for forward communication and the remaining 32 wavelengths for backward communication. On the other hand, each link in the CLOS-4PAM PNoC uses 32 DWDM wavelengths at 1.6nm channel spacing, with 16 wavelengths for forward communication and 16 wavelengths for backward communication. We use the signal power loss models presented in [9] to determine the worst-case power loss in the CLOS-OOK PNoC. For the CLOS-4PAM PNoC, we add the 4.8dB power penalty related to 4-PAM signaling to the worst-case power loss obtained for the CLOS-OOK PNoC, same as done in [10].

B. Evaluation Setup

We modeled and performed simulation based analysis of the CLOS-OOK and CLOS-4PAM PNoCs using a cycle-accurate NoC simulator, for a 256 core single-chip architecture at 22nm. We generated 100 PV maps to evaluate MR aging impact on these PNoCs for different PV profiles. We used real-world traffic from applications in the PARSEC benchmark suite [27]. GEM5 full-system simulation [28] of parallelized PARSEC applications was used to generate traces that were fed into our cycle-accurate NoC simulator. We set a "warm-up" period of 100 million instructions and then captured traces for the subsequent 1 billion instructions. We performed geometric calculations for a 20mm×20mm chip size, to determine lengths of photonic links in the CLOS-OOK and CLOS-4PAM PNoCs. We consider a 5 GHz clock frequency of operation for the cores. A 512-bit packet size is utilized for both CLOS PNoCs.

The static and dynamic energy consumption of electrical routers and concentrators in both CLOS PNoCs is based on results from the open source DSENT tool [29]. We extended the photonic model of the DSENT tool before use to include the OOK and 4-PAM signaling methods, same as in [10]. For energy consumption of photonic devices, we use 0.42pJ/bit for every modulation and detection event and 0.18pJ/bit for the driver circuits of modulators and photodetectors. We used 15% laser wall-plug efficiency and -20dBm OOK detector sensitivity to estimate the photonic laser power and correspondingly the electrical laser power from the worst-case signal power loss analysis described in previous section. We considered the DAC-based implementation of 4-PAM signaling, as described in [10], for our CLOS-4PAM PNoC.

C. Modeling of Process Variations in MRs

We adapt the VARIUS tool [30] to model die-to-die (D2D) as well as within-die (WID) process variations in MRs for the CLOS PNoC. We consider a 256-core chip with die size 400mm^2

at a 22nm process node. For the VARIUS tool, we use the parameters and procedures given in [23] and [25] to generate 100 process variation (PV) maps, each containing over 1 million points indicating the PV-induced resonance shift of MRs. The total number of points picked from these maps equal the number of MRs in the CLOS PNoC.

D. Modeling of Signal Degradation Related Power Penalty

We adopt the VBTI aging models and initial parameters defining MR characteristics from [9] for our evaluation. We compensate for the VBTI aging induced resonance red shifts using localized trimming method. To model the additional broadening of MR passbands caused by localized trimming, we use the models presented in [25]. Moreover, we adopt the equations from [19] to simulate the intermodulation crosstalk effect for both the CLOS-OOK and CLOS-4PAM PNoCs. Furthermore, we adopt the models presented in [21] to simulate the heterodyne crosstalk and signal sidelobes truncation effects for the CLOS-OOK PNoC. We also extend these models from [21], to simulate the heterodyne crosstalk and signal sidelobes truncation effects for the CLOS-4PAM PNoC, same as done in [10]. Our simulations of the intermodulation crosstalk, heterodyne crosstalk, and signal sidelobes truncation effects provide total signal power penalty as a result, which we add to our worst-case signal power loss evaluation to consequently analyze the total power consumption and energy-efficiency (in terms of energy-per-bit) of the CLOS-OOK and CLOS-4PAM PNoCs.

E. Evaluation Results

Our first set of evaluations compares the worst-case signal losses of the baseline CLOS-OOK and CLOS-4PAM PNoCs with their variants that undergo 1 Year, 3 Years, and 5 Years of VBTI aging. We have performed this aging analysis across 100 PV maps as explained in Section V-C, after the PV-induced and VBTI aging induced resonance drifts are compensated for using localized trimming. The presented results are averaged across the PV maps. Furthermore, we performed this analysis at the highest possible on-chip temperature of 357 K [31].

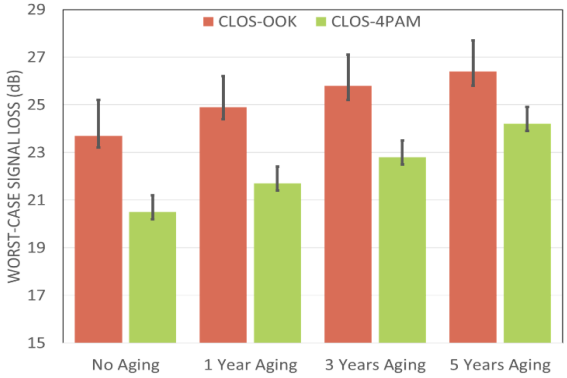

Fig. 9: Worst-case signal power loss for CLOS-OOK and CLOS-4PAM PNoCs, with 1 Year, 3 Years, and 5 Years of aging across 100 PV maps.

Fig. 9 compares the worst-case signal loss of baseline CLOS-OOK and CLOS-4PAM PNoCs with three variants of these PNoCs that undergo 1 Year, 3 Years and 5 Years of VBTI aging. The confidence intervals represent the variation in signal loss across the 100 PV maps considered. From Fig. 9, it can be observed that compared to their respective baselines, the CLOS-OOK PNoC with 1 Year, 3 Years, and 5 years of VBTI aging has 1.2dB, 2.1dB, and 2.7dB higher signal losses, and the CLOS-4PAM PNoC has 1.2dB, 2.3dB, and 3.7dB higher signal losses. As explained in Section III, the VBTI aging and use of localized trimming in MRs cause signal power attenuation due to the crosstalk effects, which in turn increases the worst-case signal power loss in the CLOS PNoCs. Moreover, it can also be observed that the CLOS-4PAM PNoC with 1 Year, 3 Years, and 5 Years of VBTI aging has 3.2dB, 3dB, and 2.2dB less signal losses compared to the CLOS-OOK PNoC with 1 Year, 3 Years, and 5 Years of VBTI aging, respectively. The relaxed channel spacing for the CLOS-4PAM PNoC reduces the spectral effects of VBTI aging, which in turn results in less signal power loss for the CLOS-4PAM PNoC with aging than the CLOS-OOK PNoC.

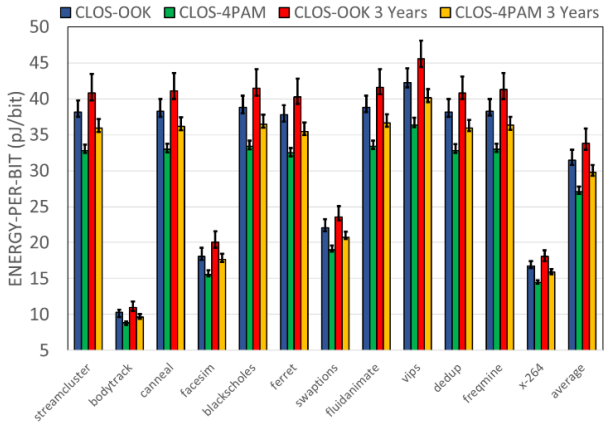

Fig. 10: Energy-per-bit (EPB) comparison of the baseline CLOS-OOK and CLOS-4PAM PNoCs with their variants with 3 Years of VBTI aging considering 100 PV maps across PARSEC benchmarks.

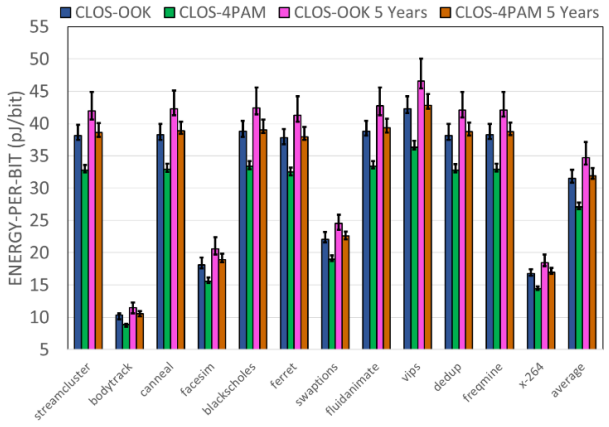

Fig. 11: Energy-per-bit (EPB) comparison of the baseline CLOS-OOK and CLOS-4PAM PNoCs with their variants with 5 Years of VBTI aging considering 100 PV maps across PARSEC benchmarks.

Fig. 10 presents energy-per-bit (EPB) results for the baseline CLOS-OOK and CLOS-4PAM PNoCs along with their variants with 3 Years of VBTI aging. Results are shown for twelve multi-threaded PARSEC benchmarks. It is evident that on average, CLOS-OOK PNoC with 3 Years of VBTI aging has 7.5% and CLOS-4PAM PNoC with 3 Years of VBTI aging has 10% higher EPB compared to their respective baselines with no aging. Similarly, Fig. 11 presents EPB results for the baseline CLOS-OOK and CLOS-4PAM PNoCs along with their variants with 5 Years of VBTI aging. Results are shown for twelve multi-threaded PARSEC benchmarks. It is evident that on average,

CLOS-OOK PNoC with 5 Years of VBTI aging has 10.3% and CLOS-4PAM PNoC with 5 Years of VBTI aging has 18% higher EPB compared to their respective baselines with no aging. The increase in the signal power loss with VBTI aging increases total laser power consumption in PNoCs, which in turn increases the EPB values for PNoCs with aging.

Moreover, it can also be observed from Fig. 9 and Fig. 10 that the CLOS-4PAM PNoC with 3 Years of VBTI aging has 0.9dB less worst-case signal power loss and 5.5% less EPB compared to the baseline CLOS-OOK without aging. The relaxed channel spacing for 4-PAM signaling based PNoCs provide proactive guard against the adverse spectral effects of VBTI aging. Therefore, 4-PAM based PNoCs can undergo up to 3 Years of aging and still achieve better energy-efficiency compared to OOK based PNoCs with no aging.

VI. CONCLUSIONS

This paper presents frequency-domain analysis of the adverse impacts of VBTI aging on photonic links and PNoCs. Our analysis identifies three key spectral effects of VBTI aging at the link-level, namely intermodulation crosstalk, heterodyne crosstalk, and signal sidelobes truncation. These spectral effects cause signal degradation and can reduce the energy-efficiency of PNoCs in terms of energy-per-bit by up to 10.3% over a span of 5 years. Moreover, our frequency-domain analysis shows that the use of 4-PAM signaling instead of traditional OOK signaling can proactively reduce signal degradation caused by aging induced spectral effects. Our system-level evaluation results indicate that 4-PAM based PNoCs can undergo 3 Years of aging and still achieve 5.5% better energy-efficiency compared to OOK based PNoCs with no aging. Thus, these results corroborate the excellent capabilities of 4-PAM signaling based PNoC architectures to proactively mitigate VBTI aging impacts.

ACKNOWLEDGMENT

This research is supported by grants from the College of Engineering, University of Kentucky and NSF (CCF-1813370).

REFERENCES

[1] W. J. Dally, B. Towles, “Route packets, not wires,” in IEEE/ACM DAC, 2001.

[2] Y. A. Vlasov et al., “Silicon CMOS-integrated nanophotonics for computer and data communications beyond 100G,” IEEE Comm. Mag., vol. 50, no. 2, pp. 67–72, Feb. 2012.

[3] J. D. Owens et al., “Research challenges for on-chip interconnection networks,” in IEEE Micro, Sep-Oct 2007.

[4] A. Joshi et al., “Silicon-photonic clos networks for global on-chip communication,” in ACM/IEEE NOCS, 2009.

[5] S. V. R. Chittamuru, S. Desai, and S. Pasricha, “A reconfigurable silicon-photonic network with improved channel sharing for multicore architectures,” in ACM GLSVLSI, 2015.

[6] S. Pasricha and S. Bahirat, “OPAL: A Multi-Layer Hybrid Pho-tonic NoC for 3D ICs,” in IEEE/ACM ASPDAC, Jan. 2011.

[7] S. Bahirat and S. Pasricha, “METEOR: Hybrid Photonic Ring-Mesh Network-on-Chip for Multicore Architectures,” in ACM JETC, vol. 13, no. 3, 2014.

[8] I. Thakkar, S. V. R. Chittamuru, and S. Pasricha, “A compara-tive analysis of front-end and back-end compatible silicon pho-tonic on-chip interconnects,” in ACM/IEEE SLIP, June 2016.

[9] S. V. R. Chittamuru, I. Thakkar, and S. Pasricha, “Analyzing Voltage Bias and Temperature Induced Aging Effects in Photonic Interconnects for Manycore Computing,” in ACM/IEEE SLIP, June 2017.

[10] I. Thakkar, S. V. R. Chittamuru, and S. Pasricha, “Improving the Reliability and Energy-Efficiency of High-Bandwidth Pho-tonic NoC Architectures with Multilevel Signaling,” in IEEE NOCS, Oct 2017.

[11] P. Dong et al., “Low Vpp, ultralow-energy, compact, high-speed silicon electro-optic modulator,” in Optics Express, vol. 17, pp. 22484–22490, 2009.

[12] Lumerical Solutions Inc. – DEVICE toolkit. https://www.lumerical.com/tcad-products/device/

[13] K. Preston et al., “Performance guidelines for WDM interconnects based on silicon microring resonators”, IEEE CLEO, 2011.

[14] M. A. Alam et al., “A comprehensive model for PMOS NBTI degradation,” Microelectronics Reliability, vol. 45, pp. 71-81, 2005.

[15] H. Kufluoglu, “MOSFET degradation due to negative bias temperature instability (NBTI) and hot carrier injection (HCI) and its implications for reliability-aware VLSI design,” PhD thesis, Purdue University, 2007.

[16] H. Kufluoglu, et al., “Theory of interface-trap-induced NBTI degradation for reduced cross section MOSFETs,” IEEE TED, 2006.

[17] J. Ahn et al., “Devices and architectures for photonic chip-scale integration”, Applied Physics A: MSP, vol. 95, pp. 989–997, 2009.

[18] C. Nitta, et al., “Addressing system-level trimming issues in on-chip nanophotonic networks,” in IEEE HPCA, 2011.

[19] K. Padmaraju et al., “Intermodulation Crosstalk Characteristics of WDM Silicon Microring Modulators,” in IEEE PTL, vol. 26, no. 14, 2014.

[20] M. Bahadori, “Optimization of Microring-based Filters for Dense WDM Silicon Photonic Interconnects”, in IEEE OI, 2015.

[21] M. Bahadori et al., “Crosstalk Penalty in Microring-Based Silicon Photonic Interconnect Systems”, JLT, vol. 34, no. 17, pp. 4043-4052, 2016.

[22] S. V. R. Chittamuru, I. Thakkar, and S. Pasricha, “Process Variation Aware Crosstalk Mitigation for DWDM based Photonic NoC Architectures,” in IEEE ISQED, Mar. 2016.

[23] S. V. R. Chittamuru, I. Thakkar, and S. Pasricha, “PICO: Miti-gating Heterodyne Crosstalk Due to Process Variations and In-termodulation Effects in Photonic NoCs,” in IEEE/ACM DAC, Jun. 2016.

[24] I. Thakkar, S. V. R. Chittamuru, and S. Pasricha, “Mitigation of Homodyne Crosstalk Noise in Silicon Photonic NoC Architec-tures with Tunable Decoupling,” in ACM CODES+ISSS, Oct. 2016.

[25] S. V. R. Chittamuru, I. Thakkar, and S. Pasricha, “HYDRA: Heterodyne Crosstalk Mitigation with Double Microring Reso-nators and Data Encoding for Photonic NoCs,” in IEEE TVLSI, vo1. 26, no. 1, 2018.

[26] I. Thakkar, S. V. R. Chittamuru, and S. Pasricha, "Run-Time Laser Power Management in Photonic NoCs with On-Chip Semiconductor Optical Amplifiers," in IEEE/ACM NOCS, 2016.

[27] C. Bienia, S. Kumar, J. P. Singh, and K. Li, “The PARSEC Benchmark Suit: Characterization and Architectural Implica-tions,” in IEEE PACT, Oct. 2008.

[28] N. Binkert et al.,"The gem5 Simulator," in CA News, May 2011.

[29] C. Sun et al., “DSENT - a tool connecting emerging photonics with electronics for opto-electronic networks-on-chip modeling,” in IEEE/ACM NOCS, 2012.

[30] S. Sarangi et al., “Varius: A model of process variation and resulting timing errors for microarchitects,” IEEE TSM, vol. 21, no. 1, 2008.

[31] M. Cho et al., “Power Multiplexing for Thermal Field Management in Many-Core Processors,” in IEEE TCPMT, vol. 3, no. 1, 2013.

[32] S. V. R. Chittamuru, I. Thakkar, S. Pasricha, “LIBRA: Thermal and Process Variation Aware Reliability Management in Photonic Networks-on-Chip,” in IEEE TMSCS, 2018.